AIAA JOURNAL
Vol. 30, No. 8, August 1992

Numerical Method for Predicting Transition in Three-Dimensional Flows by Spatial Amplification Theory

Tuncer Cebeci* and Hsun H. Chen†
California State University, Long Beach, Long Beach, California 90840

An efficient second-order-accurate numerical method, based on Keller's box scheme, is used to solve the Orr-Sommerfeld equation for three-dimensional incompressible flows. Transition is computed with the e^n method and with an eigenvalue formulation based on the saddle-point method of Cebeci and Stewartson. The frequencies needed in transition calculations are obtained from zarfs that correspond to three-dimensional neutral stability curves. The calculation method is evaluated in terms of experimental data on a swept wing and a prolate spheroid at an angle of incidence. In general, the results are in good agreement with measured values.

I. Introduction

THE prediction of transition from laminar to turbulent flow remains one of the unsolved problems of fluid mechanics. The subject is important in many applications, and this is highlighted by the needs of the National Aerospace Plane (NASP) and the High-Speed Civil Transport (HSCT) under consideration by major airframe companies. The only possibility for a general prediction method in the near future is the e^n method based on the solution of the linearized stability equations. An alternate approach, which offers exciting possibilities, is direct simulation in which the unsteady Navier-Stokes equations are solved. The excellent review of Kleiser and Zang[1] describes the rapid progress in this methodology and shows that the prediction of transition can already be achieved in some simple flows. The computer requirements of direct simulation, however, are large, and it is unlikely that it can be used for transition calculations on complex bodies in the immediate future.

A fundamental problem in the prediction of transition by stability theory is that disturbances that propagate through the boundary layer are correctly determined. The location of the onset of transition depends on the direction, magnitude, and rate of growth of these disturbances, and this information is represented by the wave numbers α and β which form a wave number vector $\boldsymbol{k}$ at an angle γ to the flow direction. One approach that is favored by Malik[2] and Mack[3] assumes a relationship between α and β, and the nature of the assumptions depends on whether spatial or temporal stability theory is used. A second approach, formulated by Cebeci and Stewartson,[4] makes use of the saddle-point method to obtain α and β and solves the Orr-Sommerfeld equation

$$\phi^{iv} - 2(\alpha^2+\beta^2)\phi'' + (\alpha^2+\beta^2)^2\phi - iR(\alpha\bar{u}+\beta\bar{w}-\omega) \times [\phi'' - (\alpha^2+\beta^2)\phi] + iR(\alpha\bar{u}''+\beta\bar{w}'')\phi = 0 \quad (1)$$

subject to boundary conditions

$$y = 0, \qquad \phi = \phi' = 0 \quad (2a)$$

$$y \to \infty, \qquad (D^2 - \xi_1^2)\phi + (\xi_1+\xi_2)(D+\xi_1)\phi = 0 \quad (2b)$$

$$(D+\xi_2)(D^2-\xi_1^2)\phi = 0 \quad (2c)$$

where $Re(\xi_1)$ and $Re(\xi_2) > 0$,

$$\xi_1^2 = \alpha^2 + \beta^2 \quad (3a)$$

$$\xi_2^2 = \alpha^2 + \beta^2 + iR(\alpha\bar{u}_e + \beta\bar{w}_e - \omega) \quad (3b)$$

with the requirement that $\partial\alpha/\partial\beta$ is real, as follows from concepts of group velocity. Whereas the assumptions used in the first approach reduce the complexity of the procedure for solving the stability equations, the more general second approach increases the complexity of the solution procedure since the solution of the eigenvalue problem is more demanding.

Until 1964, the numerical methods used to solve Eq. (1) for two-dimensional flows where $\beta = 0$ and $\bar{w} = 0$ made use of initial-value schemes and were limited to the range of lower Reynolds numbers. The integration procedure usually started at the edge of the boundary layer where the asymptotic solutions of the stability equation are of the form,

$$\phi = A_1 \exp(-\xi_1 y) + A_2 \exp(-\xi_2 y) \quad (4)$$

with ξ_1 and ξ_2 given by

$$\xi_1^2 = \alpha^2, \qquad \xi_2^2 = \alpha^2 + iR(a\bar{u}_e - \omega) \quad (5)$$

The two independent solutions of Eq. (4) grow at different rates, one of them [associated with $\exp(-\xi_1 y)$] slowly, and the other [associated with $\exp(-\xi_2 y)$] rapidly. Even though the solutions are linearly independent at the beginning, with increasing Reynolds number they become linearly dependent as the solutions progress to the wall due to contamination of the slower-growing solutions by the faster-growing solutions. Multiple precision can alleviate this difficulty at moderate Reynolds numbers but is unable to overcome the parasitic error growth at higher Reynolds numbers. Kaplan[5] devised a scheme where the slowly growing solution was purified from its parasitic error at each integration step so that, at the end of the integration interval, the solution was not dominated by the faster-growing solution, and this was found to be successful in solving the Orr-Sommerfeld equation at Reynolds numbers up to $R_{\delta^*}(\equiv u_e\delta^*/\nu) = 10^4$.

Presented as Paper 91-1606 at the AIAA 22nd Fluid Dynamics, Plasma Dynamics, and Lasers Conference, Honolulu, HI, June 24-26, 1991; received July 29, 1991; revision received Jan. 20, 1992; accepted for publication Jan. 24, 1992.

*Professor and Chairman, Aerospace Engineering Department. Fellow AIAA.

†Associate Professor, Aerospace Engineering Department. Senior Member AIAA.

Wazzan et al.[6] applied Kaplan's technique to the Orr-Sommerfeld equation and solved it with the Gram-Schmidt orthogonalization procedure to obtain accurate solutions for a wide range of Reynolds numbers, including incompressible flows with heat transfer. The main shortcoming is the eigenvalue procedure, which is cumbersome, especially in heat transfer problems, and leads to high computer times as well as to a breakdown of the solutions when the initial estimates of the eigenvalues are not close to the final answer.

In general, finite difference methods do not have the problems associated with the parasitic error growth and have been successfully used in recent years to solve the stability equation, including flows at high Reynolds numbers. A popular scheme is that based on a matrix finite difference method used by Srokowski and Orszag[7] for three-dimensional incompressible flows and by Malik[2] for compressible flows. Another successful finite difference method is that based on Keller's box scheme, which has been used extensively for two- and three-dimensional boundary-layer flows.[8] This method is used here to solve Eq. (1) with an eigenvalue formulation based on the saddle-point method. It is described in the following section and used to determine the location of the onset of transition in three-dimensional flows with the e^n method. The results, which include comparisons with measurements on wings and bodies of revolution, are presented in Sec. III. The paper ends with a summary of the more important conclusions.

II. Numerical Method

The definitions

$$\xi_2^2 = \xi_1^2 + iR(\alpha\bar{u} + \beta\bar{w} - \omega) \tag{6a}$$

$$\xi_3 = iR(\alpha\bar{u}'' + \beta\bar{w}'') \tag{6b}$$

in addition to the one given by Eq. (3a) allow Eq. (1) to be written in the compact form:

$$\phi^{iv} - \xi_1^2\phi'' - \xi_2^2(\phi'' - \xi_1^2\phi) + \xi_3\phi = 0 \tag{7}$$

To formulate the numerical scheme with Keller's box method, we reduce Eqs. (7) and (2) to an equivalent first-order system. We define

$$\phi' = f \tag{8a}$$

$$f' = s + \xi_1^2\phi \tag{8b}$$

$$s' = g \tag{8c}$$

and write Eq. (7) as

$$g' = \xi_2^2 s - \xi_3\phi \tag{8d}$$

With the new variables, the boundary conditions of Eqs. (2) become

$$y = 0, \qquad \phi = 0, \qquad f = 0 \tag{9a}$$

$$y = \delta, \qquad s + (\xi_1 + \xi_2)f + \xi_1(\xi_1 + \xi_2)\phi = 0 \tag{9b}$$

$$g + \xi_2 s = 0 \tag{9c}$$

where ξ_2, defined by Eq. (6a), attains its value at $y = \delta$ and is identical to the expression defined by Eq. (3b).

We now consider a nonuniform mesh with $y = \delta$ represented by y_J, denote the quantities (f, s, g, ϕ) at points y_j by (f_j, s_j, g_j, ϕ_j) and write the finite difference approximations of Eqs. (8) for the midpoint $y_{j-1/2}$ using centered-difference derivatives

$$\phi_j - \phi_{j-1} - c_3(f_j + f_{j-1}) = (r_1)_j = 0 \tag{10a}$$

$$f_j - f_{j-1} - c_3(s_j + s_{j-1}) - c_1(\phi_j + \phi_{j-1}) = (r_3)_{j-1} = 0 \tag{10b}$$

$$s_j - s_{j-1} - c_3(g_j + g_{j-1}) = (r_2)_j = 0 \tag{10c}$$

$$g_j - g_{j-1} - c_4(s_j + s_{j-1}) - c_2(\phi_j + \phi_{j-1}) = (r_4)_{j-1} = 0 \tag{10d}$$

Here, with h_{j-1} denoting $y_j - y_{j-1}$,

$$c_3 = \frac{h_{j-1}}{2}, \quad c_1 = \xi_1^2 c_3, \quad c_2 = -(\xi_3)_{j-1/2}c_3, \quad c_4 = (\xi_2^2)_{j-1/2}c_3 \tag{11}$$

Equations (11) are imposed for $j = 1, 2, \ldots, J$, and additional boundary conditions follow from Eqs. (9) and can be written as

$$\phi_o = (r_1)_o = 0, \qquad f_o = (r_2)_o = 0 \tag{12a}$$

$$f_J + c_3 s_J + c_1\phi_J = (r_3)_J = 0$$
$$g_J + c_4 s_J = (r_4)_J = 0 \tag{12b}$$

where now

$$c_3 = \frac{1}{\xi_1 + (\xi_2)_J}, \qquad c_1 = \xi_1, \qquad c_4 = (\xi_2)_J \tag{13}$$

Since the Orr-Sommerfeld equation and its boundary conditions are homogenous, the trivial solutions $f_j = s_j = \phi_j = g_j = 0$ $(0 \le j \le J)$ are valid for all values of α, β, ω, and R. For this reason, in order to compute the eigenvalues and the eigenfunctions, we first replace the boundary condition $\phi'(0) = 0$ (that is, $f_o = 0$) of Eqs. (12) by $\phi''(0) = 1$, that is, $s_o = 1$. Now the difference equations have a nontrivial solution since $\phi''(0) \neq 0$, and we seek to adjust or to determine parameter values so that the original boundary condition is satisfied. This is achieved by an iteration scheme based on Newton's method. Specifically, we first write Eqs. (10), the wall boundary conditions

$$\phi_o = (r_1)_o = 0, \qquad s_o = (r_2)_o = 1 \tag{14}$$

and the edge boundary conditions in Eq. (12b) in matrix-vector form, that is,

$$\mathcal{A}\,\underset{\approx}{\delta} = \underset{\approx}{r} \tag{15}$$

where

$$\mathcal{A} = \begin{bmatrix} A_o & C_o & & & & & \\ B_1 & A_1 & C_1 & & & & \\ & \cdot & \cdot & \cdot & & & \\ & & B_j & A_j & C_j & & \\ & & & \cdot & \cdot & \cdot & \\ & & & & B_{J-1} & A_{J-1} & C_{J-1} \\ & & & & & B_J & A_J \end{bmatrix} \tag{16a}$$

$$\underset{\approx}{\delta} = \begin{bmatrix} \underset{\sim}{\delta}_0 \\ \vdots \\ \underset{\sim}{\delta}_j \\ \vdots \\ \underset{\sim}{\delta}_J \end{bmatrix}, \qquad \underset{\approx}{r} = \begin{bmatrix} \underset{\sim}{r}_0 \\ \vdots \\ \underset{\sim}{r}_j \\ \vdots \\ \underset{\sim}{r}_J \end{bmatrix} \tag{16b}$$

$$\underset{\sim}{\delta}_j = \begin{bmatrix} \phi_j \\ s_j \\ f_j \\ g_j \end{bmatrix}, \qquad \underset{\sim}{r}_j = \begin{bmatrix} (r_1)_j \\ (r_2)_j \\ (r_3)_j \\ (r_4)_j \end{bmatrix} \tag{16c}$$

and the A_j, B_j, C_j denote 4×4 matrices given by

$$A_o \equiv \begin{bmatrix} 1 & 0 & 0 & 0 \\ 0 & 1 & 0 & 0 \\ (c_1)_1 & (c_3)_1 & 1 & 0 \\ (c_2)_1 & (c_4)_1 & 0 & 1 \end{bmatrix}$$

$$A_j \equiv \begin{bmatrix} 1 & 0 & -(c_3)_j & 0 \\ 0 & 1 & 0 & -(c_3)_j \\ (c_1)_{j+1} & (c_3)_{j+1} & 1 & 0 \\ (c_2)_{j+1} & (c_4)_{j+1} & 0 & 1 \end{bmatrix}, \quad 1 \le j \le J-1$$

$$A_J = \begin{bmatrix} 1 & 0 & -(c_3)_J & 0 \\ 0 & 1 & 0 & -(c_3)_J \\ (c_1)_{J+1} & (c_3)_{J+1} & 1 & 0 \\ 0 & (c_4)_{J+1} & 0 & 1 \end{bmatrix}$$

$$B_j = \begin{bmatrix} -1 & 0 & -(c_3)_j & 0 \\ 0 & -1 & 0 & -(c_3)_j \\ 0 & 0 & 0 & 0 \\ 0 & 0 & 0 & 0 \end{bmatrix}, \quad 1 \le j \le J$$

$$C_j = \begin{bmatrix} 0 & 0 & 0 & 0 \\ 0 & 0 & 0 & 0 \\ (c_1)_{j+1} & (c_3)_{j+1} & -1 & 0 \\ (c_2)_{j+1} & (c_4)_{j+1} & 0 & -1 \end{bmatrix}, \quad 0 \le j \le J-1 \tag{17}$$

We note from the difference equations defined by Eqs. (10), (12b), and (14) that the solution of Eq. (15) depends on the four parameters α, β, ω, and R, and we can denote this dependence by writing

$$\underset{\approx}{\delta} = \underset{\approx}{\delta}(\alpha, \beta, \omega, R) \tag{18}$$

Recalling that α and β are complex, and that ω is real in spatial-amplification theory, the preceding relation implies that the solution of Eq. (15) depends on six scalars (α_r, α_i, β_r, β_i, ω, and R). With any four of these scalars fixed, we can compute the remaining two scalars in such a way that the missing boundary condition $\phi'(0) = 0$ is satisfied. In our finite difference notation, this corresponds to the condition

$$f_o(\alpha, \beta, \omega, R) = 0 \tag{19}$$

This requires the establishment of a relationship between the two complex wave numbers α and β if ω and R are fixed. In our method, this relationship is provided by the saddle-point method, which leads to the requirement

$$\left(\frac{\partial \alpha}{\partial \beta}\right)_{\omega, R} = -\tan \gamma \tag{20}$$

where γ is real and denotes the direction of the propagation of the disturbance. We shall use this requirement to solve the Orr-Sommerfeld equation so that transition can be computed with the e^n method. Before we discuss the solution procedure, however, it is useful to recall that the calculation of critical Reynolds number R_{cr} is of fundamental importance to stability theory. In two-dimensional flows, associated with R_{cr} are the neutral curves on which α is real. It may be expected that in three-dimensional flows a neutral curve can be found for any chosen value of β/α as a curve in the three-dimensional space of α, ω, R, but in general it will not penetrate to values of R as low as R_{cr}. Only for one value of β/α will this lower bound be achieved. One possible choice is the envelope of the neutral curve, which we may think of as the absolute neutral curve, in that it is independent of β/α, or to give it a short evocative name we shall follow the suggestion of Cebeci and Stewartson[4] and define it as the zarf (lit. envelope, Turk.). This curve passes through the critical point in α, β, ω, R space at which $R = R_{cr}$ and turns out to be of significant importance in the calculation of transition as we shall discuss later in the paper.

A. Zarf

The zarf has a number of interesting properties of which the most important is that along the zarf

$$\alpha_i = \beta_i = 0, \qquad \partial\alpha/\partial\beta = \text{real} \tag{21}$$

To obtain the frequencies used in transition calculations, we compute the eigenvalues of the zarf for a fixed R. For this purpose we write Eq. (19) as

$$f_o(\alpha, \beta, \omega) = 0 \tag{22}$$

Since α_i and β_i are zero on the zarf, Eq. (22) contains three unknowns (α_r, β_r, ω) and an additional equation based on Eq. (20) is needed. It can be obtained by first expanding Eq. (22) with ω constant,

$$df = \left(\frac{\partial f}{\partial \alpha}\right)_\beta d\alpha + \left(\frac{\partial f}{\partial \beta}\right)_\alpha d\beta = 0 \tag{23}$$

Solving Eq. (23) for $d\alpha/d\beta$ we get

$$\left(\frac{d\alpha}{d\beta}\right)_\omega = -\frac{(\partial f/\partial \beta)}{(\partial f/\partial \alpha)} = e \tag{24}$$

Expanding Eq. (22) about (α^ν, β^ν, ω^ν) and retaining only the linear terms in the expansion and after separating the real and imaginary parts of the resulting expression, we get

$$f_r^\nu + \left(\frac{\partial f_r}{\partial \alpha}\right)^\nu \delta\alpha + \left(\frac{\partial f_r}{\partial \beta}\right)^\nu \delta\beta + \left(\frac{\partial f_r}{\partial \omega}\right)^\nu \delta\omega = 0 \tag{25a}$$

$$f_i^\nu + \left(\frac{\partial f_i}{\partial \alpha}\right)^\nu \delta\alpha + \left(\frac{\partial f_i}{\partial \beta}\right)^\nu \delta\beta + \left(\frac{\partial f_i}{\partial \omega}\right)^\nu \delta\omega = 0 \tag{25b}$$

Similar to Eq. (22) we now expand Eq. (24) to obtain

$$e^\nu + \left(\frac{\partial e}{\partial \alpha}\right)^\nu \delta\alpha + \left(\frac{\partial e}{\partial \beta}\right)^\nu \delta\beta + \left(\frac{\partial e}{\partial \omega}\right)^\nu \delta\omega = 0 \tag{26}$$

Since we are interested in the values of α, β, and ω for which the imaginary part of ($d\alpha/d\beta$) or e_i is zero, from Eq. (26) we can write

$$e_i^\nu + \left(\frac{\partial e_i}{\partial \alpha}\right)^\nu \delta\alpha + \left(\frac{\partial e_i}{\partial \beta}\right)^\nu \delta\beta + \left(\frac{\partial e_i}{\partial \omega}\right)^\nu \delta\omega = 0 \tag{27}$$

Solution of Eqs. (25) and (27) allows us to write $\delta\alpha$, $\delta\beta$, and $\delta\omega$ as

$$\delta\alpha = \frac{1}{\Delta_1}\left[-f^r(f_\beta^i e_\omega^i - f_\omega^i e_\beta^i) + f^i(f_\beta^r e_\omega^i - e_\beta^i f_\omega^r) - e^i(f_\beta^r f_\omega^i - f_\omega^r f_\beta^i)\right] \tag{28a}$$

$$\delta\beta = \frac{1}{\Delta_1}\left[f_\alpha^r(-f^i e_\omega^i + e^i f_\omega^i) - f_\alpha^i(-f^r e_\omega^i + e^i f_\omega^r) + e_\alpha^i(-f^r f_\omega^i + f^i f_\omega^r)\right] \tag{28b}$$

$$\delta\omega = \frac{1}{\Delta_1}\left[f_\alpha^r(-f_\beta^i e^i + f^i e_\beta^i) - f_\alpha^i(-f_\beta^r e^i + f^r e_\beta^i) + e_\alpha^i(-f_\beta^r f^i + f^r f_\beta^i)\right] \tag{28c}$$

$$\Delta_1 = e_\alpha^i(f_\beta^r f_\omega^i - f_\beta^i f_\omega^r) - e_\beta^i(f_\alpha^r f_\omega^i - f_\alpha^i f_\omega^r) + e_\omega^i(f_\alpha^r f_\beta^i - f_\alpha^i f_\beta^r) \tag{29}$$

Here for simplicity we have dropped the superscripts ν and $\nu+1$ and denoted the real and imaginary parts of f, $f_\alpha(\equiv \partial f/\partial\alpha)$, $f_\beta(\equiv \partial f/\partial\beta)$, $f_\omega(\equiv \partial f/\partial\omega)$, $e_\alpha(\equiv \partial e/\partial\alpha)$, $e_\beta(\equiv \partial e/\partial\beta)$, $e_\omega(\equiv \partial e/\partial\omega)$ by superscripts r and i. We note from Eq. (27) that if $\delta\alpha$, $\delta\beta$, and $\delta\omega$ are all zero, then e_i is zero and e is real.

To calculate the derivative of e with respect to α, β and ω, we make use of Eq. (24). For example, rewriting Eq. (24) as

$$e = -\frac{f_\beta}{f_\alpha} \tag{30}$$

and differentiating it with respect to β, we get

$$e_\beta = -\frac{f_{\beta\beta}}{f_\alpha} + \frac{f_\beta}{f_\alpha^2} f_{\alpha\beta} \tag{31a}$$

Similarly,

$$e_\alpha = -\frac{f_{\beta\alpha}}{f_\alpha} + \frac{f_\beta}{f_\alpha^2} f_{\alpha\alpha} \tag{31b}$$

$$e_\omega = -\frac{f_{\beta\omega}}{f_\alpha} + \frac{f_\beta}{f_\alpha^2} f_{\alpha\omega} \tag{31c}$$

We note from Eqs. (28) and (31) that the calculation of $\delta\alpha$, $\delta\beta$, and $\delta\omega$ also requires the calculation of $f_{\alpha\beta}$, $f_{\alpha\alpha}$, $f_{\beta\omega}$, $f_{\beta\beta}$, and $f_{\alpha\omega}$. They can be obtained by differentiating Eq. (15) with respect to appropriate eigenvalues. For example, to find the eigenfunction $f_{\alpha\beta}$, we differentiate Eq. (15) first with respect to α then with respect to β:

$$\mathcal{A}\left(\frac{\partial^2 \underset{\approx}{\delta}}{\partial\alpha\partial\beta}\right)^\nu = -\frac{\partial \mathcal{A}}{\partial\beta}\left(\frac{\partial \underset{\approx}{\delta}}{\partial\alpha}\right)^\nu - \frac{\partial \mathcal{A}}{\partial\alpha}\left(\frac{\partial \underset{\approx}{\delta}}{\partial\beta}\right)^\nu - \frac{\partial^2 \mathcal{A}}{\partial\alpha\partial\beta}\underset{\approx}{\delta}^\nu \tag{32}$$

Equation (32) is the variational equation of Eq. (15) with respect to α and β. Thus, to obtain the required derivative $f_{\alpha\beta}$, Eq. (32) has to be solved with the same coefficient matrix $\mathcal{A}$ already computed and factored for Eq. (15). The vectors on the right-hand side of Eq. (32) are determined from Eqs. (10), (12), and (14). Note that eigenfunctions f_α and f_β are obtained from the solutions of the variational equations with respect to α and β, that is,

$$\mathcal{A}\left(\frac{\partial \underset{\approx}{\delta}}{\partial\alpha}\right)^\nu = -\left(\frac{\partial \mathcal{A}}{\partial\alpha}\right)\underset{\approx}{\delta}^\nu, \quad \mathcal{A}\left(\frac{\partial \underset{\approx}{\delta}}{\partial\beta}\right)^\nu = -\left(\frac{\partial \mathcal{A}}{\partial\beta}\right)\underset{\approx}{\delta}^\nu \tag{33}$$

To find the variational equations with respect to $\alpha\alpha$, $\alpha\beta$, $\beta\beta$, $\alpha\omega$, and $\beta\omega$, we follow a similar procedure. For example, to find those for $\alpha\alpha$, we differentiate Eq. (15) twice with respect to α

$$\mathcal{A}\left(\frac{\partial^2 \underset{\approx}{\delta}}{\partial\alpha^2}\right)^\nu = -2\frac{\partial \mathcal{A}}{\partial\alpha}\left(\frac{\partial \underset{\approx}{\delta}}{\partial\alpha}\right)^\nu - \frac{\partial^2 \mathcal{A}}{\partial\alpha^2}\underset{\approx}{\delta}^\nu \tag{34}$$

To summarize one step of the calculation of the eigenvalues of the zarf, we first solve Eq. (15) for initial estimates of α, β, and ω, which we obtain with a continuation method described in Sec. II.A. If the computed value of f_o does not satisfy Eq. (22), then we solve appropriate variational equations to calculate the increments in α, β, and ω from Eqs. (28) so that we can obtain new estimates of α, β, and ω that will satisfy Eq. (22) and will make e real. This procedure is repeated until convergence. Since the eigenvalue formulation is based on Newton's method, our calculations usually indicate quadratic convergence.

B. Estimation of Eigenvalues

The solution of Eq. (22) requires initial estimates of the eigenvalues and, since Newton's method is used to compute the subsequent estimates, it is desirable to have good estimates. A convenient procedure advocated by Keller and sometimes referred to as the continuation method is described in the following for this purpose. It is general and can also be used for flows in which the velocity profiles change rapidly from one x station to another.

We define

$$\begin{aligned}
\bar{u} &= \bar{u}_{\text{ref}} + n(\bar{u} - \bar{u}_{\text{ref}}) \\
\bar{w} &= \bar{w}_{\text{ref}} + n(\bar{w} - \bar{w}_{\text{ref}}) \\
\bar{u}'' &= \bar{u}''_{\text{ref}} + n(\bar{u}'' - \bar{u}''_{\text{ref}}) \\
\bar{w}'' &= \bar{w}''_{\text{ref}} + n(\bar{w}'' - \bar{w}''_{\text{ref}})
\end{aligned} \tag{35}$$

Here $\bar{u}$ and $\bar{w}$ correspond to the velocity profiles of the flow under consideration at a Reynolds number R, and $\bar{u}_{\text{ref}}$ and $\bar{w}_{\text{ref}}$

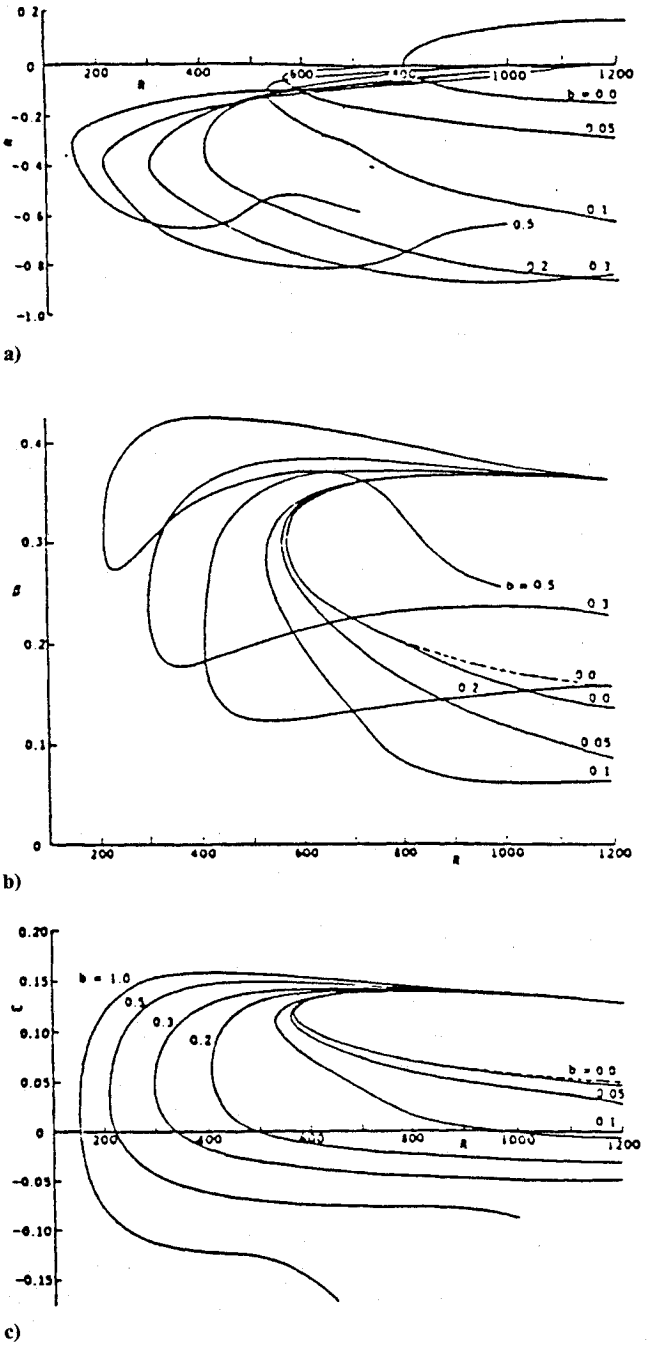

Fig. 1 Zarfs for the leading edge of a wing for several values of b: dashed lines indicate two-dimensional neutral curves for attachment line flow.

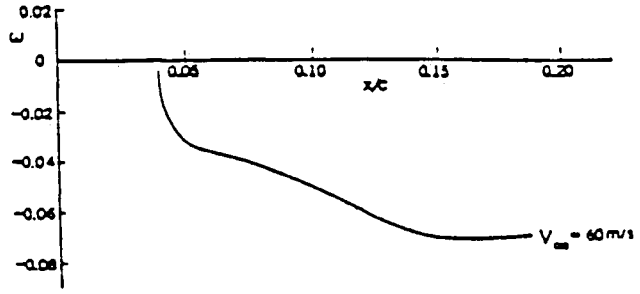

Fig. 2 Variation of ω on zarf near the leading edge of the ONERA-D wing: $\lambda = 49$ deg; $V_\infty = 60$ ms^{-1}; $\alpha = 0$ deg.

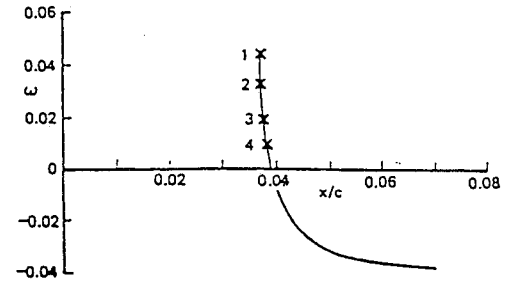

Fig. 3 Variation of ω on zarf very close to the leading edge of the ONERA-D wing for $\alpha = 0$ deg and $V_\infty = 60$ ms^{-1}.

denote reference velocity profiles with a Reynolds number R_{ref} and with eigenvalues of α_0, β_0, and ω_0. The parameter n is a sequence of specified numbers ranging from 0 to 1 and it follows from Eqs. (35) that the profiles $\bar{u}$, $\bar{w}$, and $\bar{u}''$, $\bar{w}''$ correspond to the reference profiles for $n = 0$ and to those for which eigenvalues α, β, and ω are to be determined at specified R for $n = 1$.

In general, the reference Reynolds number is different from the flow Reynolds number so that it may be desirable to obtain the initial estimates of the eigenvalues α, β, and ω of the reference velocity profiles at the desired Reynolds number R. Again, this can conveniently be done by the continuation method in which the Reynolds number R is varied according to

$$R = R_{\text{ref}} + n(R - R_{\text{ref}}) \tag{36}$$

with initial estimates of α, β, and ω corresponding to α_o, β_o, ω_o at $R = R_{\text{ref}}$ and subsequent values of α, β, and ω for each value of n coming from the previous value of n. Care should be taken, however, to ensure that the critical Reynolds number of either profile is less than the flow Reynolds number.

To calculate the eigenvalues of the reference velocity profiles, we make use of zarfs for the leading edge of a yawed wing for several values of $b = u_e / w_e$. To discuss this point further, we consider a three-dimensional laminar flow near the leading edge of a yawed wing in which the freestream velocity is represented by V_∞ and the sweep angle by λ. Denoting the chordwise and spanwise components of V_∞ by u_∞ and w_e, we can write

$$u_\infty = V_\infty \cos\lambda, \qquad w_e = V_\infty \sin\lambda \tag{37}$$

Near the leading edge of a yawed wing where $u_e = Ax$, the boundary-layer equations admit similarity solutions, and with the use of the Falkner-Skan transformation[9]

$$\eta = \sqrt{u_e/\nu x}\, y, \qquad \psi = \sqrt{u_e \nu x}\, f(x,\eta) \tag{38}$$

and with $f' = u/u_e$, $g' = w/w_e$, they can be expressed as

$$f''' + ff'' - (f')^2 + 1 = 0, \qquad g''' + fg'' = 0 \tag{39}$$

subject to

$$f = f' = g = g' = 0 \qquad \text{at} \quad \eta = 0$$

$$f' \to 1, \qquad g' \to 1 \qquad \text{as} \quad \eta \to \infty \tag{40}$$

Equation (1) has been written in dimensionless form so that all velocities and lengths are normalized by a reference velocity u_o and length l and the Reynolds number R is defined by $R = u_o l/\nu$. The radian frequency ω is made dimensionless by dividing the physical frequency ω^* by u_o/l, primes denote differentiation with respect to a dimensionless distance $\bar{y} = (y/l)$, and the wave numbers α and β are normalized by the reference length l. For the flow under consideration, it is useful to define the length scale by $l = \sqrt{\nu/A}$ and choose the characteristic velocity in the Orr-Sommerfeld equation to be w_e so that the Reynolds number in Eq. (1) can be defined by $R = \sqrt{R_x}/b$ where

$$R_x = \frac{u_e x}{\nu}, \qquad b = \frac{u_e}{w_e} = \frac{u_e \cot\lambda}{u_\infty} \tag{41}$$

With the choice of the same length and velocity scales in the boundary-layer and stability equations, the Orr-Sommerfeld equation can be solved without interpolating the velocity profiles $\bar{u}$ and $\bar{w}$, which are obtained from $\bar{u} = bf'$ and $\bar{w} = g'$.

Figure 1 shows zarfs for various values of b for which $b = 0$ represents the attachment-line flow along the stagnation line of the yawed wing. In this case, it may appear that α is equal to zero for all Reynolds numbers but, as was reported for the Blasius flow in Ref. 8, bifurcation also occurs for this flow on the lower branch at $R = 8 \times 10^2$ where $\omega = 0.07$. The value of α is zero for $R < 8 \times 10^2$, and becomes finite and varies with R as shown in Fig. 1a. Figures 1b and 1c show the variation of β and ω with R, respectively, and as in Fig. 1a, they provide the appropriate limits of zarfs with $b > 0$ for transition calculations. It is useful to note that the main differences between the neutral curve with $\alpha = 0$ and the zarf are in α and β so that β changes by 0.110 at $R = 1.4 \times 10^3$, while ω changes only by 0.0032.

As in the case of the Blasius flow,[10] the attachment-line flow solutions for the zarf approach a finite limit on the lower branch as $R \to \infty$, and to confirm this, we follow the procedure described in Ref. 10. With subscript 2 denoting the two-dimensional form of the Orr-Sommerfeld equation, we consider Eq. (1) and write

$$|\alpha| = B, \qquad \beta R = BR_2, \qquad \omega R = \omega_2 R_2$$

and let $R \to \infty$ holding B, R_2, and ω_2 fixed. The resulting equation with $b = 0$ can then be written as

$$\phi'''' - 2B^2\phi'' + B^4\phi = iR_2(B\bar{w} - \omega_2)[\phi'' - B^2\phi] - iBR_2\bar{w}''\phi$$

i.e., the two-dimensional form. We now use the equivalent two-dimensional definition of the zarf to obtain the values of B, R_2, and ω_2 and minimize $\omega_2 R_2$ on the neutral stability curve. In this case, the minimum value of $\omega_2 R_2$ occurs at $R_2 = 795$ and $B = 0.2025$ and is 55.81. Hence, on the lower branch of the zarf

$$|\alpha| \to 0.2025, \qquad \beta R \to 161.0, \qquad \omega R \to 55.81$$

and they are in good agreement with our calculations for large values of R. For example, at $R = 1.5 \times 10^4$,

$$|\alpha| = 0.2017, \qquad \beta = 0.01074, \qquad \omega = 0.003720$$

such that $\beta R = 161.1$, $\omega R = 55.8$

The zarfs in Fig. 1 indicate that, although for a given value of b all three eigenvalues α, β, and ω are relatively flat away from the critical Reynolds number, they vary significantly

near the critical Reynolds number. Perhaps the most interesting feature of these curves is the behavior of the dimensionless frequency as a function of R. Although they are relatively flat at higher Reynolds numbers for a given value of b, they vary considerably near the critical value of R. In particular, they change from a negative value to a positive value on the lower branch and suggest that in determining the critical frequency in the e^n method care must be taken in the choice of step lengths used in the boundary layer and subsequently in the stability calculations. A relatively large Δx spacing can lead to critical frequencies that do not necessarily lead to maximum amplification rates and, as a result, to an inaccurate calculation of transition location by the e^n method. We shall discuss this point further in Sec. III.

C. Transition Prediction

In two-dimensional stability calculations using spatial amplification theory, the onset of transition is computed by evaluating the integral

$$n = -\int_{x_0}^{x} \alpha_i \, dx \tag{42}$$

for a set of specified dimensional frequencies $\omega^*/2\pi$. With the velocity profiles $\bar{u}$ and its second derivative $\bar{u}''$, obtained from the solution of the laminar boundary-layer equations, the solutions of the Orr-Sommerfeld equation reduces to an eigenvalue problem involving four scalar quantities α_r, α_i, R, and ω. With the value of R known at any streamwise station on the body, and with dimensional frequency specified, the real and imaginary parts of the wave number α can be computed so that transition can be calculated from Eq. (42). Usually the procedure for one frequency is repeated for different frequencies in order to find the critical frequency that leads to the most amplified integrated amplification rate. For attached flows, it is not common to search for the critical frequency but to determine it from the envelope procedure. However, for flows with separation, the envelope procedure does not apply, and it is necessary to search for the critical frequency.

Our method for computing transition in three-dimensional flows is similar to that for two-dimensional flows in that we use the zarf to determine the frequency needed in the transition calculations. For a specified dimensional frequency and Reynolds number, we compute the eigenvalues α and β so that transition can be computed from Eq. (42) with α_i replaced by Γ, which denotes the amplification rate defined by

$$\Gamma = \alpha_i - \beta_i \left(\frac{\partial \alpha}{\partial \beta}\right)_{\omega,R} = \alpha_i - \beta_i e_r \tag{43}$$

With ω known and e_r fixed [equal to its value at zarf, say (x_1, z_1)], Eq. (15) is solved for initial estimates of α and β to get a solution at (x_2, z_2). To obtain the next values of α and β, we use Newton's method in which we expand f_o and e in Eqs. (22) and (24),

$$f_o + \left(\frac{\partial f}{\partial \alpha}\right)_o \delta\alpha + \left(\frac{\partial f}{\partial \beta}\right)_o \delta\beta = 0 \tag{44a}$$

$$e_o + \left(\frac{\partial e}{\partial \alpha}\right)_o \delta\alpha + \left(\frac{\partial e}{\partial \beta}\right)_o \delta\beta = e = \text{given} \tag{44b}$$

Solving for $\delta\alpha$ and $\delta\beta$, we get

$$\delta\alpha = -\frac{1}{\Delta_o}\left[f_o e_\beta + f_\beta (e - e_o)\right] \tag{45a}$$

$$\delta\beta = \frac{1}{\Delta_o}\left[f_\alpha (e - e_o) + f_o e_\alpha\right] \tag{45b}$$

where

$$\Delta_o a = f_\alpha e_\beta - f_\beta e_\alpha \tag{46}$$

As before, f_α, f_β, e_α, and e_β are determined by solving the variational equations with respect to α, β, $\alpha\alpha$, $\alpha\beta$, and $\beta\beta$. This procedure is repeated until $\delta\alpha$ and $\delta\beta$ are less than a specified tolerance parameter. On convergence, the amplification parameter Γ is computed from Eq. (43). Since the calculation of Γ assumes that the value of e on the right-hand side of Eq. (44b) is fixed by the value it takes on the zarf, we compute a new value of e for which Γ is minimum, and this is achieved by assigning a new value of e. After convergence, we compute Γ from Eq. (43) and test to see whether Γ is increasing or decreasing. Since a positive Γ implies that disturbances are damped, we can increment e until a minimum value of Γ is computed.

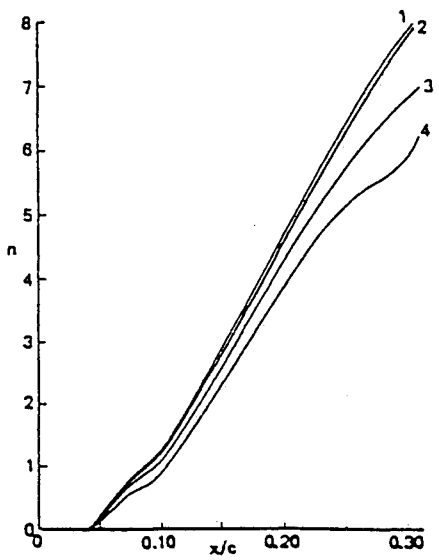

Fig. 4 Variation of the amplification factors for $\alpha = 0$ deg and $V_\infty = 60$ ms^{-1}.

III. Results and Discussion

The calculation method of the preceding section has been used to compute transition on an infinite swept wing and a body of revolution. It has also been used to investigate the effect of curvature on transition in incompressible flows[11] and has recently been extended to three-dimensional compressible flows.[12,13] In this section, we present a small sample of results for an infinite swept wing and a body of revolution and discuss the importance and usefulness of zarf calculations on transition.

A. Infinite Swept Wing

The calculations for an infinite swept wing were performed for an ONERA-D wing equipped with a cambered leading edge and attached to a half fuselage. Before we present a sample of calculations reported in Ref. 14, it is useful to discuss the procedure used to obtain the eigenvalues and to compute the dimensional frequencies needed in the e^n method. For given velocity profiles, the stability calculations began on the zarf, near the leading edge, with initial estimates of eigenvalues α and β determined from Fig. 1. Several calculations showed that the location of zarf had a pronounced effect on the location of transition and that, near the wing leading edge, the lower branch solutions of the zarf changed drastically from positive to negative. Figure 2 shows the variation of zarf near the leading edge of the ONERA-D wing for $\lambda = 49$ deg and $V_\infty = 60$ ms^{-1} at $\alpha = 0$ deg. As can be seen, the lower branch of the ω zarf is negative with relatively flat values of ω

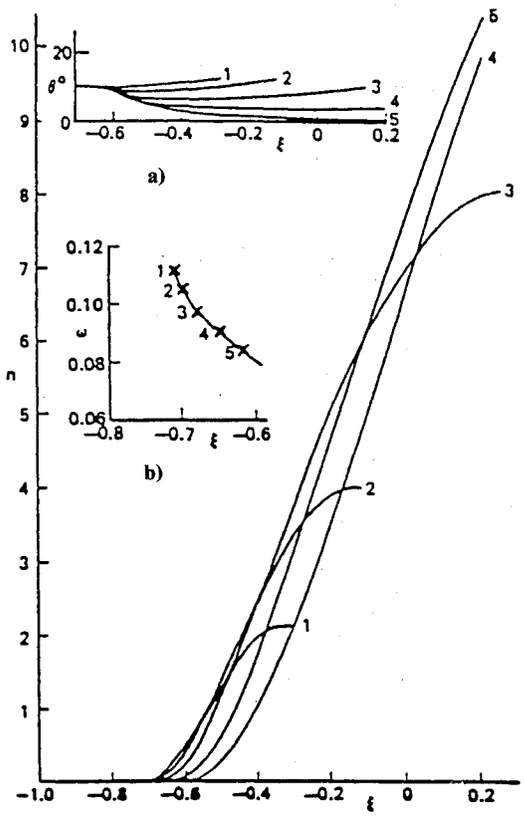

Fig. 5 Amplification factors computed with disturbances originating at $\theta = 10$ deg for five frequencies determined on the zarf (insert a) and with different wave propagation trajectories (insert b).

away from the leading edge, whereas ω undergoes a very rapid variation near $x/c = 0.04$, a behavior consistent with zarfs of Fig. 1. Figure 3 shows that ω becomes positive and increases rapidly around $x/c = 0.04$. For additional results showing the behavior of ω near the wing leading edge at different angles of attack, see Ref. 14.

On the calculation of the eigenvalues of the zarf at a specified x/c location, the calculations proceed to the next x/c station in order to solve the eigenvalue problem for α and β for specified dimensional frequencies determined on the zarf with the requirement that $\partial\alpha/\partial\beta$ is real and is given by its value at the previous x/c location. The computed values of α and β are used to calculate the amplification rate Γ, and the eigenvalue procedure is repeated for specified values of e_r in order to determine its value for which Γ is minimum. Once determined, the calculations proceed to the next x/c station in order to compute new values of α, β so that another minimum value of Γ can be determined. The calculations for the experimental arrangement of Ref. 15 indicate that it is important to vary e_r in order to maximize the amplification rate Γ and that failure to specify the direction of the disturbance with minimum Γ produces unacceptable results.

This procedure is for one value of frequency chosen at a certain x/c location and is repeated for different values of ω computed for a zarf at different x/c locations. Since the frequency near the leading edge of the wing varies drastically, it is important to choose these x/c locations carefully. Figure 4 shows the integrated amplification rates for four different frequencies in Fig. 3. As can be seen, the computed amplification rates originate almost at the same x/c location and amplify differently depending on the choice of the frequency and may give different predictions of transition location if the frequency is not chosen carefully.

The accuracy of this procedure for computing transition was investigated for 13 cases of which seven were for a sweep angle $\lambda = 49$ deg, three were for $\lambda = 55$ deg, and three were for $\lambda = 61$ deg. The calculations, which are summarized in Ref. 14, are in excellent agreement with experimental data.

B. Prolate Spheroid

The calculations for a prolate spheroid were performed at an incidence angle of 10 deg and were compared with the experimental data of Meier and Kreplin.[16] Reference 14 describes the calculation procedure and presents results for the windward and leeward lines of symmetry as well as those off the line of symmetry. In principle, the calculation of transition on the lines of symmetry is somewhat similar to the calculation of transition in two-dimensional flows and is not described here. Off the line of symmetry, the flow is three dimensional and, in general, the circumferential wave number β is not equal to zero. In addition, unlike the flow over an infinite swept wing, the flow cannot be assumed sectionally similar in either streamwise or circumferential direction. As a result, as eigenvalues α and β are being computed to obtain the amplification rates for a specified dimensional frequency, wave angle, e_r, and ξ location, the variation of the velocity profiles u and $\bar{w}$ in the circumferential direction must also be accounted for.

Figure 5 shows the integrated amplification rates with disturbances originating at $\theta = 10$ deg for five frequencies determined on the zarf and with their wave propagation trajectories varying as shown in insert b. Of these, the frequencies denoted by 4 and 5 correspond to the critical values, and the wave with a frequency of 5 causes transition on the line of symmetry at $\xi = 0.20$, ahead of the wave that originated on the line of symmetry (discussed in Ref. 14) and causes transition to occur after $\xi = 0.30$. The disturbance with frequency 4 also causes transition. However, in this case it takes place off the line of symmetry at $\xi = 0.18$. This indicates that in three-dimensional flows there can be more than one critical frequency emerging at a fixed θ location and leading to transition. For additional results for $\theta = 20$, 40, 80, 120, and 150 deg, the reader is referred to Ref. 14.

Figure 6 presents a summary of the stability/transition calculations. The first curve on the left-hand side corresponds to the location of the critical frequencies on the zarf. We note from this curve that its behavior as we approach the leeward line of symmetry begins to exhibit a difference at $\theta \geq 160$ deg

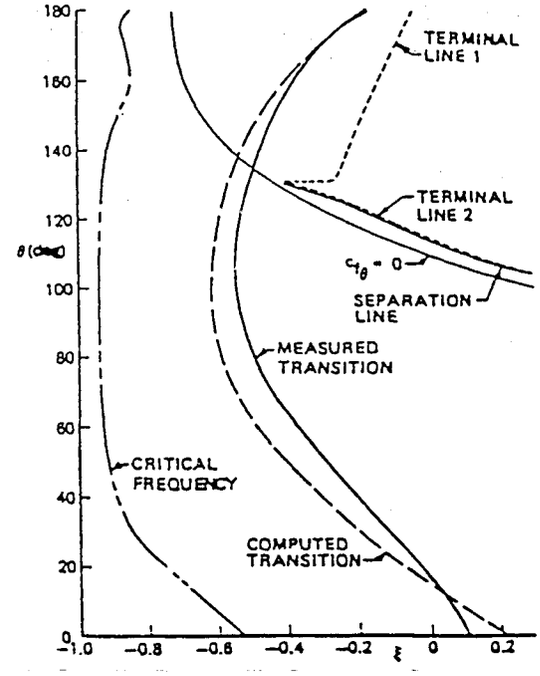

Fig. 6 Calculated and experimental transition locations on the prolate spheroid at $\alpha = 10$ deg.

from those at $\theta < 160$ deg. This difference is due to the effect of the crossflow velocity profiles, which begin to exhibit significant changes with ξ as the calculations progress downstream of the zarf. To the right of this curve is the dashed line, which corresponds to the locus of transition location computed with the present method for $n = 10$. The experimental values are denoted by the solid line to the right of this computed transition curve.

Figure 6 also presents the separation line for this angle of attack that, as in the $\alpha = 6$ deg case studied by Cebeci and Su,[17] is open and corresponds to a skin-friction line, as discussed in detail in Ref. 17. The lines referred to as the terminal lines are defined by the breakdown of the boundary-layer calculations which, in this case, correspond to the vanishing of the streamwise wall shear. This, as discussed in Ref. 14, is due to the formulation of the boundary-layer problem in direct form and can be avoided by the use of inverse procedures in which the external velocities are computed as part of the solution.

IV. Concluding Remarks

A numerical method for solving the Orr-Sommerfeld equation for three-dimensional incompressible flows is described. The eigenvalue procedure is formulated so that the relationship between the two wave numbers is determined as part of the computational method. The usefulness of the neutral stability curves (zarfs) for the critical frequency and its location needed in the e^n method has been clearly demonstrated for three-dimensional flows. In particular, the zarfs facilitate the determination of critical frequencies and avoid uncertainties associated with the choice of their magnitude and location.

The application of the numerical method to two flows corresponding to an infinite swept wing and a prolate spheroid shows that the method is efficient and accurate, and the use of the continuation method allows the stability calculations to be performed without any numerical difficulties, even in cases where the velocity profiles change drastically from one location to another.

References

[1]Kleiser, L., and Zang, T. A., "Numerical Simulation of Transition in Wall Bounded Shear Flows," *Annual Review of Fluid Mechanics,* Vol. 23, 1991, pp. 495–537.

[2]Malik, M. R., "COSAL—A Black-Box Compressible Stability Analysis Code for Transition Prediction in Three-Dimensional Boundary Layers," NASA CR 165952, 1982.

[3]Mack, L. M., "Stability of Three-Dimensional Boundary-Layers on Swept Wings at Transonic Speeds," International Union of Theoretical and Applied Mechanics Symposium, Transsonicum 111, Göttingen, Germany, May 1988.

[4]Cebeci, T., and Stewartson, K., "Stability and Transition in Three-Dimensional Flow," *AIAA Journal,* Vol. 18, No. 4, 1980, pp. 398–405.

[5]Kaplan, R. E., "The Stability of Laminar Incompressible Boundary Layers in the Presence of Compliant Boundaries," Massachusetts Inst. of Technology, Aero-Elastic and Structures Research Lab. Rept., ASRL-TR-116-1, 1964.

[6]Wazzan, A. R., Okamura, T. T., and Smith, A. M. O., "Spatial and Temporal Stability Charts for the Falkner-Skan Boundary Profiles," Douglas Aircraft Co., Rept. DAC-67D86, 1968.

[7]Srokowski, A., and Orszag, S. A., "Mass Flow Requirements for LFC Wing Design," AIAA Paper 77-1222, 1977.

[8]Bradshaw, P., Cebeci, T., and Whitelaw, J. H., *Engineering Calculation Methods for Turbulent Flows,* Academic Press, London, 1981.

[9]Cebeci, T., and Bradshaw, P., *Physical and Computational Aspects of Convective Heat Transfer,* Springer-Verlag, NY, 1988.

[10]Cebeci, T., and Stewartson, K., "Asymptotic Properties of the Zarf," *AIAA Journal,* Vol. 19, No. 6, 1981, pp. 806–807.

[11]Cebeci, T., Chen, H. H., and Kaups, K., "Further Consideration of the Effect of Curvature on the Stability of Three-Dimensional Flows," *Computer & Fluids,* (to be published).

[12]Cebeci, T., Khattab, A. A., Chen, H. H., and Chen, L. T., "An Approach to the Design of Wings: the Role of Mathematics, Physics and Economics," AIAA Paper 92-0286, Jan. 1992.

[13]Niethammer, R., Arnal, D., deLaharpe, V., Chen, H. H., and Cebeci, T., "Three-Dimensional Compressible Stability-Transition Calculations Using the Spatial Theory," *Proceedings of the Fifth Symposium on Numerical and Physical Aspects of Aerodynamic Flows,* California State University, Long Beach, CA, Jan. 1992.

[14]Cebeci, T., Chen, H. H., Arnal, D., and Huang, T. T., "A Three-Dimensional Linear Stability Approach to Transition on Wings and Bodies of Revolution at Incidence," *AIAA Journal,* Vol. 29, No. 12, 1991, pp. 2077–2085.

[15]Arnal, D., and Juillian, J. C., "Three-Dimensional Transition Studies at ONERA/CERT," AIAA Paper 87-1335, 1987.

[16]Meier, H. U., and Kreplin, H. P., "Experimental Investigation of the Boundary-Layer Transition on a Body of Revolution," *Zeitschrift fuer Flugwiss Weltraumforsch,* Vol. 4, 1981, p. 65.

[17]Cebeci, T., and Su, W., "Separation of Three-Dimensional Laminar Boundary Layers on a Prolate Spheroid," *Journal of Fluid Mechanics,* Vol. 181, 1988, pp. 47–77.